Variability of Indonesian throughflow within Makassar Strait, 2004–2009

R. Dwi Susanto,[1] Amy Ffield,[2] Arnold L. Gordon,[1] and T. Rameyo Adi[3]

Received 29 March 2012; revised 26 July 2012; accepted 30 July 2012; published 13 September 2012.

[1] In contrast to earlier measurements, January 2004 through May 2009 Makassar Strait velocities within the main Pacific inflow pathway of the Indonesian throughflow (ITF) are larger with a clear signal of the Asian-Australian monsoon overriding the relatively weak 2006/2007 El Niño and 2007/2008 La Niña. The Makassar flow is thermocline intensified with maximum along-channel velocity of −0.8 m/s near 120 m during the southeast monsoon, July to September, decreasing to −0.6 m/s from October to December, during the transition to the northwest monsoon. The temperature variability is highly correlated to ENSO, and the salinity variability reveals low-salinity surface water inputs to the ITF, possibly from the Java and Sulu seas. Empirical Orthogonal Function (EOF) analysis of the velocity profile reveals that the first mode (45%) is dominated by the intrusions of Kelvin waves from the south, the second mode (30%) reflects ENSO modulation, and the third mode (17%) is associated with regional monsoon winds. The strength of the northward intrusions of Kelvin waves plays an important role in the total transport. The 2004–2009 average seasonal transport varied from −15.5 Sv (Sv = 10^6 m^3/s) during the northwest monsoon (January to March) to −9.6 Sv during the monsoon transition (October to December). The annual mean transport is southward at 13.3 ± 3.6 Sv, with small year-to-year range from 12.5 to 14.0 Sv, substantially higher than measurements from 1997 when El Niño suppressed the transport (9.2 Sv).

Citation: Susanto, R. D., A. Ffield, A. L. Gordon, and T. R. Adi (2012), Variability of Indonesian throughflow within Makassar Strait, 2004–2009, *J. Geophys. Res.*, *117*, C09013, doi:10.1029/2012JC008096.

1. Introduction

[2] With a diverse assortment of ocean passages and basins, the Indonesian seas provide a circuitous route for tropical Pacific water to flow into the Indian Ocean, in what is referred to as the Indonesian throughflow (ITF). The tendency for the ITF to pass through the western-most available passages in the Indonesian seas (Figure 1), establishes the Makassar Strait as the primary inflow path of the Pacific water [*Wajsowicz*, 1996]. However, deeper inflow ITF components, blocked by the 680 m Dewakang Sill in the southern Makassar Strait [*Gordon et al.*, 2003a], pass through an eastern path by way of the Maluku Sea [*Gordon and Fine*, 1996; *van Aken et al.*, 2009]. In addition, there is a smaller inflow branch of the ITF, the South China Sea throughflow originating from the Luzon Strait, which flows into the shallow Java Sea via Karimata Strait [*Fang et al.*, 2005, 2010; *Susanto et al.*, 2010], and into the Sulu and Sulawesi seas via the Mindoro Strait and the Sibutu Passage [*Gordon et al.*, 2012]. The South China Sea throughflow may influence the vertical structure of the main ITF [*Fang et al.*, 2005, 2009; *Gordon et al.*, 2003b; *Tozuka et al.*, 2007, 2009].

[3] The first simultaneous measurements of various ITF streams was obtained by the collaborative effort of scientists from the countries of Indonesia, Australia, Netherlands, France and the United States, during the INSTANT program (International Nusantara Stratification and Transport Program) in 2004–2006 [*Gordon et al.*, 2010; *Sprintall et al.*, 2004]. Under the INSTANT program 11 moorings measuring ocean currents, temperature and salinity were deployed at major inflow-passages in the Makassar Strait and Lifamatola Passage, and major outflow-passages in the Lombok Strait, Ombai Strait and Timor passage (Figure 1). While the start and end date of individual moorings varied, the INSTANT program simultaneously observed the major ITF passages over a 3-year period from January 2004 to December 2006. A brief description of the Makassar Strait throughflow observed during INSTANT is presented by *Gordon et al.* [2008]. When the INSTANT program ended in 2006, a single mooring in the Makassar Strait was redeployed, and then recovered in May 2009. In this paper, we present the analysis of nearly 5.5 years of observational data in the

[1]Lamont-Doherty Earth Observatory, Columbia University, Palisades, New York, USA.
[2]Physical Oceanography, Earth & Space Research, Upper Grandview, New York, USA.
[3]Research and Development Agency for Marine and Fisheries, Jakarta, Indonesia.

Corresponding author: R. D. Susanto, Lamont-Doherty Earth Observatory, Columbia University, 61 Rte. 9W, Palisades, NY, 10964 USA. (dwi@ldeo.columbia.edu)

0148-0227/12/2012JC008096

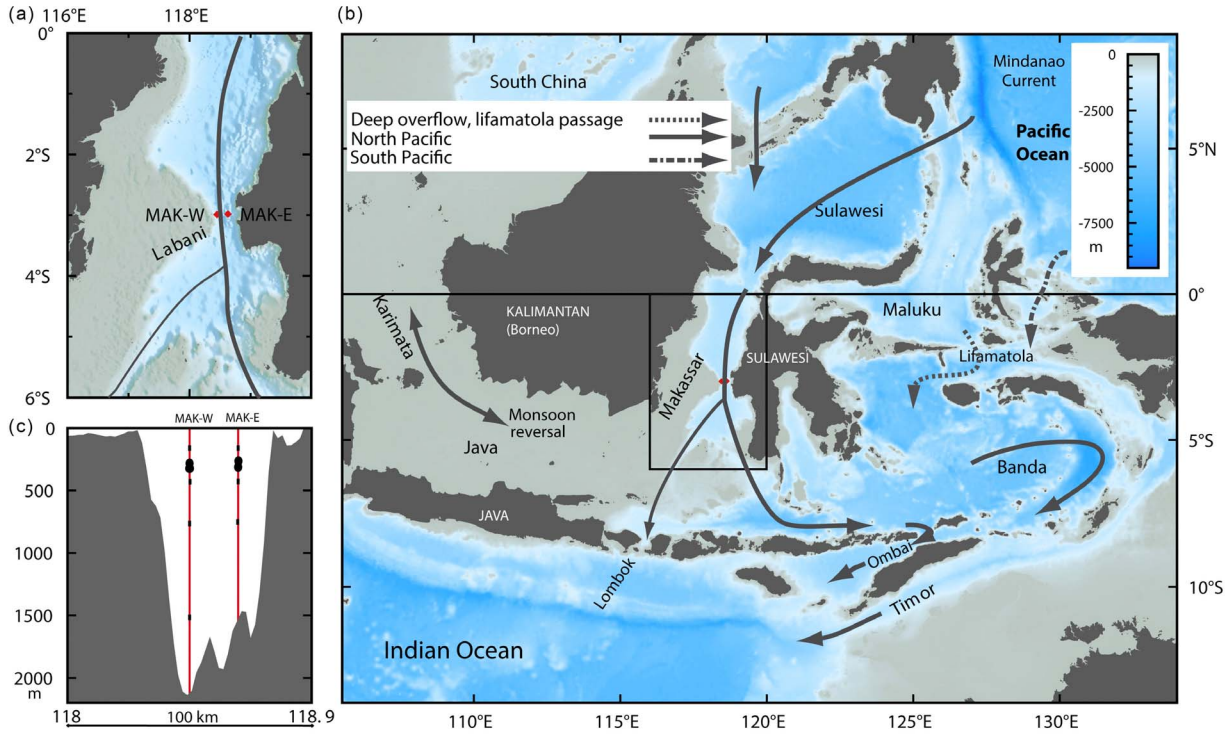

Figure 1. (b) The ITF pattern modified from *Gordon and Fine* [1996]. The double arrowhead line between Java and Kalimantan represent the seasonal reversal of the Karimata Strait throughflow [*Fang et al.*, 2010; *Susanto et al.*, 2010]. (a) The black box, encompassing Makassar Strait, is enlarged, showing as red dots the INSTANT MAK-west and MAK-east mooring locations within the 45 km wide Labani channel constriction near 3°S for period 2004–2006. From December 2006 through May 2009, only MAK-west has been redeployed to monitor the ITF in the Makassar Strait. (c) Positions of current meters and ADCP are shown on the mooring lines in the cross-section.

Makassar Strait including both the INSTANT and the post-INSTANT Makassar data for the combined time period, 18 January 2004 to 31 May 2009 (for brevity, the time period is henceforth referred to as 2004–2009).

[4] Because the geographic location of Indonesia straddles the equator between the Pacific and Indian Oceans, and between two continents, Australia and Asia, the ITF is affected by a complex interplay between local and remote ocean and atmospheric forcing from both the Pacific and the Indian Oceans, such as tides, the Madden-Julian Oscillation, Kelvin and Rossby waves, the Asian-Australian monsoon, the El Niño Southern Oscillation (ENSO), and the Indian Ocean Dipole (IOD) [i.e., *England and Huang*, 2005; *McCreary et al.*, 2007; *Meyers*, 1996; *Saji et al.*, 1999; *Webster et al.*, 1999]. The ITF is highly variable across a broad range of frequencies from tidal, intraseasonal, seasonal and interannual time scales, including monsoonal variability: The northwest monsoon occurs from November to March and the southeast monsoon occurs from May to September, with the transition months in April and October [*Aldrian and Susanto*, 2003; *Wheeler and McBride*, 2005]. In this paper we discuss the Makassar Strait seasonal and interannual variability of velocity and transport as well as their vertical structures as observed over the 2004–2009 observational time period. The intraseasonal variability revealed by the INSTANT Makassar time series is discussed by *Pujiana et al.* [2009, 2012], while the Makassar tidal variability is described by *Robertson* [2010]. The velocity and transport time series not only reinforce the earlier 1996–1998 Arlindo and INSTANT Makassar throughflow results [*Gordon et al.*, 1999, 2008; *Susanto and Gordon*, 2005], but they also reveal a number of new major aspects of the spatial and temporal variability in the Makassar throughflow profile, illuminating the colliding forces of Pacific and Indian Ocean processes impacting the Indonesian seas.

[5] First we will present the Makassar Strait mooring configurations, and then we discuss the seasonal and interannual variability of velocity, temperature, and salinity associated with the monsoons, ENSO, and IOD. An Empirical Orthogonal Function (EOF) analysis of velocity time series is then presented followed by the Makassar Strait volume transport estimate. We conclude with a summary of the main findings.

2. Mooring Configuration and Data

[6] On 18 January 2004 the two INSTANT Makassar moorings (Figure 1), were deployed within the Labani channel of the Makassar Strait at MAK-west at 2°51.9′S, 118°27.3′E, and MAK-east at 2°51.5′S, 118°37.7′E [*Gordon et al.*, 2008]. Both MAK-west and MAK-east moorings were instrumented with an upward looking RDI Long Ranger 75 kHz Acoustic Doppler Current Profiler (ADCP) and Argos beacon, at a nominal depth of 300 m. These two

ADCPs were configured to measure all three velocity components in 10 m vertical bins at 30 min intervals. Downward looking ADCPs were mounted at both moorings at a nominal depth of 307 m. Single point current meters were mounted at the MAK-west mooring at 200 m, 400 m, 750 m and 1500 m; at the MAK-east mooring, two current meters were mounted at 400 m and 750 m. All current meters and ADCPs include temperature sensors. In addition, 15 Temperature-Pressure (TP) sensors and two conductivity-temperature-pressure (CTD) recorders were mounted at the MAK-west over the depth range of 45 m to 468 m. MAK-east was equipped with one TP sensor and two CTD recorders over the nominal depth range of 115 m to 294 m. The two moorings were recovered in late November 2006, providing good quality data for nearly 3 years during the INSTANT time period (henceforth referred to as 2004–2006).

[7] Upon recovering the INSTANT moorings, the MAK-west mooring was redeployed in late November 2006, as part of the Monitoring ITF in the Makassar Strait (MITF) program. The MAK-west mooring configuration included ADCPs and current meters, but without temperature and salinity sensors. The upward and downward looking ADCPs were mounted at the mooring at a nominal depth of 500 m and 520 m, respectively; three Aquadopp current meters were mounted at the mooring at a nominal depth of 510 m, 760 m, and 1550 m. Both downward and upward looking ADCPs and current meters provide good quality data for full depth from surface to 800 m, and at 1550 m for the entire 2.5-year time period of 29 November 2006 to 31 May 2009 (henceforth referred to as 2007–2009).

[8] Data quality control has been applied to the ADCP data, with special attention to the near surface bins of the top 10% of the ADCP measurement range, which may be contaminated by sea surface reflection. Quality of each ping at each of four beams has been checked for the percent "good," the threshold value, the velocity shear between bins and consecutive time, the echo intensity as well as the correlation magnitude.

[9] Before combining the ADCP velocity for the upper layer and deeper current meter velocity time series, an adjustment of the velocity-pressure profile is applied to account for mooring blow over by ocean currents and tides. MAK-east blow over (ranging from 289 to 513 m with a median at 335 m) was slightly less than that of MAK-west (ranging from 296 to 560 m with a median at 335 m) not only due to lesser velocity magnitude but also due to its shorter length of mooring wire above the ADCP. During 2007–2009, the MAK-west blow over ranged from 467 to 713 m with a median at 471 m. As evident in the Arlindo data [*Susanto et al.*, 2000; *Susanto and Gordon*, 2005] strong semi-diurnal and diurnal tides with significant fortnightly modulation are the most dominant features of the current meter time series. For instruments without a direct pressure recorder, pressure was derived using nearest full time series pressure record and the length of mooring wire between instruments.

[10] After applying quality control to each individual instrument time series for both MAK-west and MAK-east moorings, we decomposed current vectors into along-channel and across-channel component by rotating the velocity data parallel and perpendicular to the Labani channel. The downstream direction along the Labani Channel axis is 170° (referenced to true north). Along-channel velocity is parallel to the Labani Channel axis. Within this study, "velocity" refers to along-channel velocity, with negative values indicating flow toward 170°. The velocity time series of each mooring was compiled into a single velocity-depth time series by filtering and interpolating data onto a common time base of 2 hours. In order to resolve the subtidal velocity profile, a 2-day Lanczos low-pass filter was applied to the velocity time series [*Duchon*, 1979]. The velocity data from the ADCPs and current meters were then linearly interpolated onto a 20 m depth grid profile for the 2-hour time steps.

3. Variability of Velocity, Temperature, and Salinity

3.1. Velocity Variability

[11] The velocity time series from MAK-west span from 2004 into 2009, while that for MAK-east from 2004 to 2006 only. The velocity time series from both moorings were processed separately. Velocities of MAK-west and MAK-east are well correlated ($r > 0.9$ for the upper 750 m) and exhibit western intensification consistent with previous measurements [*Gordon et al.*, 1999, 2008; *Susanto and Gordon*, 2005] and numerical models [*Metzger et al.*, 2010; *Shriver et al.*, 2007], which may due to *beta* effect and geometry of the Labani Channel. Hence, it was determined to be reasonable and cost effective to monitor the ITF in the Makassar Strait using a single mooring after 2006; and in this paper, we present velocity variability of MAK-west from January 2004 to May 2009 (for brevity we refer to this period simply as 2004–2009). When calculating the transport (Section 5), we also present the total volume transport calculated based on an average of both MAK-west and MAK-east velocity time series from 2004 to 2006.

[12] The 2004–2009 Makassar southward maximum of sub-tidal (weekly mean) velocity attains 1.3 m/s while the northward maximum reaches 0.7 m/s. After a 1-month low-pass filter has been applied, the southward maximum velocity is 1.0 m/s while the northward maximum is 0.2 m/s (Figure 2). Figure 2a shows 3-month averaged velocity profile for January to March (JFM), April to June (AMJ), July to September (JAS), and October to December (OND). To capture the maximum ocean response, the seasonal groupings are delayed 1 month from the monsoonal winds (Figure 3). In the upper 200 m, velocity (Figures 2a and 2b) clearly exhibits thermocline intensification with maximum velocity near 120 m during the peak of the southeast monsoon (July to September). The velocity maximum scales to its depth (Figure 2c) with increased speeds as the velocity maximum shoals. Below 200 m the velocity is stronger during the northwest monsoon (JFM) than that during southeast monsoon (JAS). For the duration of the observations from 2004 to 2009, the minimum velocity within the upper 800 m occurs in October to December, marking the transition from southeast to the northwest monsoon phase.

[13] To determine annual and interannual variability, the MAK-west 2004–2009 velocity time series is separated into the mean seasonal structure (Figure 3) and its residual/interannual (Figure 4). Seasonal velocity was obtained by taking the daily mean of velocity from 2004 to 2009 to make

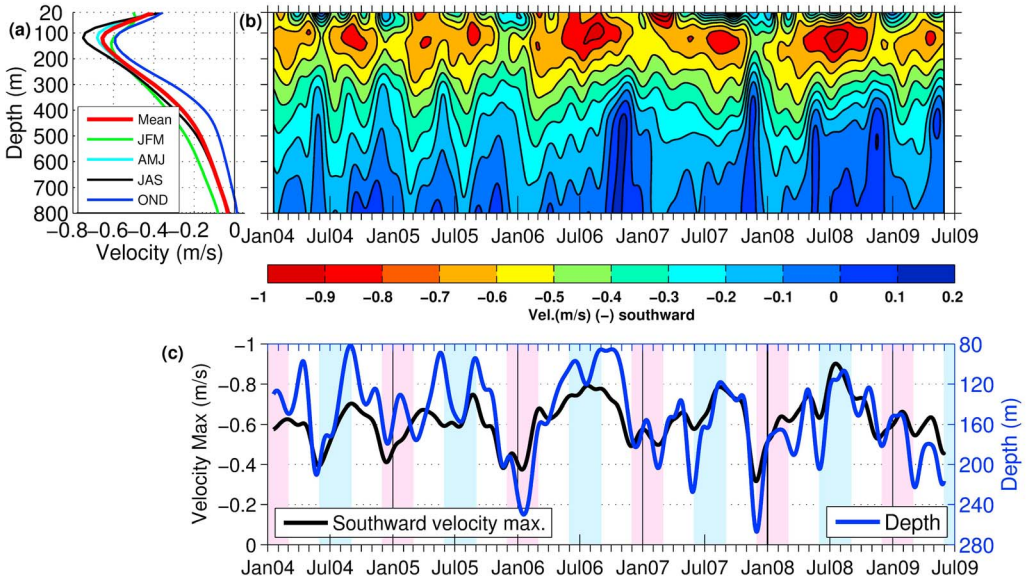

Figure 2. The Makassar Strait seasonal depth profiles of (a) velocity and (b) time series derived from the ADCP and current meter data for the period January 2004 through May 2009. For clarity in representing the figure, a monthly low-pass filter has been applied before contouring. Contour interval is 0.1 m/s. Negative values denote flow toward 170° along the Labani Channel axis. (c) The velocity maximum (black) scales to its depth (blue) reveals a relationship of increased speeds as the velocity maximum shoals. Season grouping is assumed 1-month delay from the monsoonal winds. Peak of southeast monsoon is shaded in cyan, while peak of northwest monsoon is shaded in magenta.

a daily annual time series, and then extended the data into 3 years repeating annual time series and then applied 3-month Lanczos low-pass filter to the time series. The second year time series then is assigned as the annual time series (Figure 3). The maximum seasonal flow occurs in July to September, which is about a 1-month delay of the southeast monsoon winds, with southward velocities up to 0.8 m/s. Prevailing southeasterly winds draw Makassar Strait water into the Java Sea enhancing the Makassar Strait transport [*Gordon et al.*, 2003b] and reducing the South China Sea throughflow in the Karimata Strait [*Fang et al.*, 2010]. Above 200 m the southward seasonal flow is persistently greater than 0.5 m/s, whereas below 200 m it exhibits northward flow events due to semi-annual Kelvin waves in May and November. Using mooring data from the South Java coast, wind data, and an analytical approach, *Sprintall et al.* [1999] identified the propagation of Kelvin waves from the equatorial Indian Ocean in mid-May 1997. Furthermore, using mooring data from the southern Java coast and Lombok and Makassar Straits, equatorial Indian Ocean

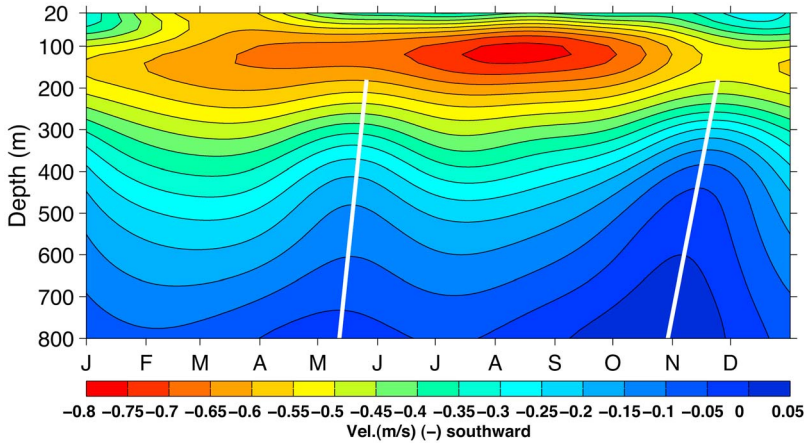

Figure 3. The 2004 to 2009 Makassar Strait mean seasonal velocity. Contour interval is 0.05 m/s. Three-month low-pass filter has been applied before contouring. Negative values denote southward flow. Maximum southward velocity occurs in July to September during the southeast monsoon (1-month delay from the southeast monsoon winds). The northward intrusions of semi-annual Kelvin waves are clearly seen in May and November at the deeper levels (white lines).

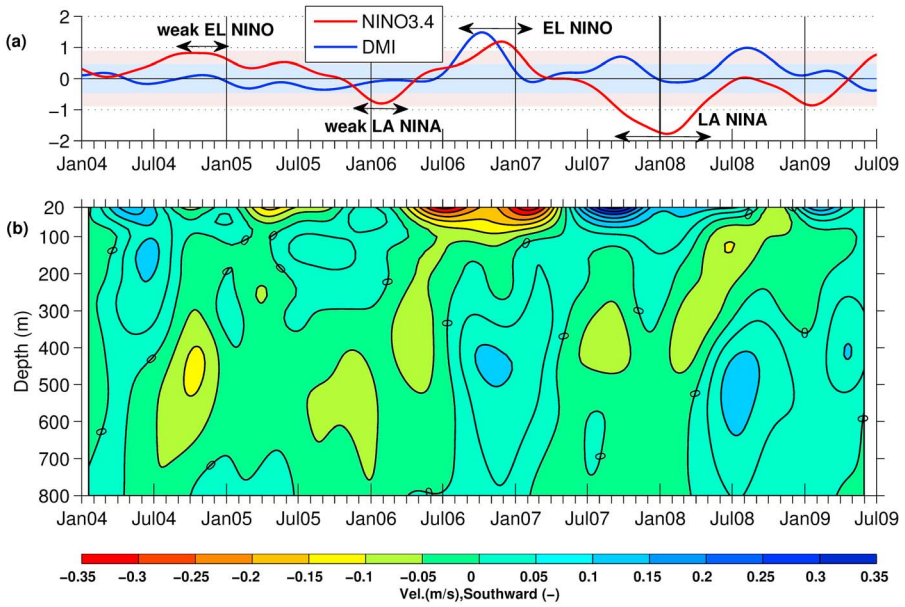

Figure 4. (a) Time series of NINO3.4 index (red) and DMI (blue). Standard deviation of NINO3.4 (shaded magenta) and DMI (shaded blue). (b) The Makassar Strait interannual variability of velocity during the observation period, January 2004 through May 2009. Six-month low-pass filter has been applied before contouring.

wind data, sea surface height data from satellite altimeter, and analytical and numerical models, *Sprintall et al.* [2000] identified the propagation of Kelvin waves along the Sumatra-Java coast entering Lombok Strait and Makassar Strait in May 1997. Using a numerical model, *Syamsudin et al.* [2004] showed that it was possible for Kelvin waves to enter the Lombok Strait toward the Makassar Strait. Semi-annual Kelvin waves were observed in INSTANT data in the outflow-passages [*Sprintall et al.*, 2009]. Recently, using a numerical model, *Shinoda et al.* [2012] showed that the coastally trapped Kelvin waves entering the Lombok Strait act to reduce the Makassar southward flow. Here, following the cores of the lowest velocities (Figure 3) associated with the Kelvin waves in May and November (velocity contours tilt to the right), the upward propagating phase or downward energy propagation [*Drushka et al.*, 2010; *McCreary*, 1984] can be estimated. For the Kelvin wave in May, the averaged upward propagating phase from 800 m to 180 m is 44 m/day while that for the Kelvin wave in November is 22 m/day.

[14] The 2004–2009 velocity time series spans the 2006/2007 El Niño with positive IOD and the 2007/2008 La Niña with neutral IOD (Figure 4a). The amplitude of the seasonal variability velocity (Figure 3) is twice that of the amplitude of the interannual variability (Figure 4b). The interannual variability was obtained by subtracting seasonal variability (Figure 3) from the velocity profile (Figure 2a) and then applied a half-year Lanczos low-pass filter. In contrast, during the Arlindo program in 1996–1998 when there was an exceptionally strong El Niño with a positive IOD event, the interannual variability was higher and suppressed the seasonal variability [*Gordon et al.*, 1999; *Susanto and Gordon*, 2005]. While interactions between these two larger forcing (ENSO and IOD) is beyond the scope of our paper, the Makassar Strait velocity reveals the effects of ENSO and IOD. Longer time series which cover more ENSO events are needed to understand interaction between ENSO and throughflow. In addition, ENSO impacts on the throughflow may vary with different type of ENSO [*Shinoda et al.*, 2011]. During 2006/2007 El Niño, the interannual forcing enhanced the southward seasonal flow in the upper 100 m surface layer, while below 100 m the interannual forcing reduced the southward flow. Conditions were reversed during the 2007/2008 La Niña.

3.2. Temperature and Salinity Variability

[15] The 2004–2006 INSTANT measurements provide a high-resolution view of the Makassar temperature profile within the thermocline, which as described above, coincides with the Makassar velocity maximum core. A total of 13 TP and four CTD instruments, all with 6-minute temperature and pressure time steps, were recovered from the MAK-west and MAK-east moorings, spanning between the nominal depths of 100 m and 468 m. By including eight temperature sensors that were bundled with the velocity instruments on the moorings, a total of 25 temperature-pressure time series were recovered altogether, spanning between the nominal depths of 100 m and 1500 m. Quality control was carried out on all 25 temperature time series to account for sensor drift or for pressure measurement failure. Robust corrections were possible because all the instruments were rigidly fastened to mooring wire and also typically had nearby functioning instruments. In the Makassar Strait, strong velocities, including tidal, force the instruments to be swept from their nominal depths, downward to deeper levels; when the velocities weaken, the instruments relax back to shallower levels. As the instruments are sampling continuously, this has the fortuitous result of profiling the water column, with multiple instruments obtaining measurements at the same depths, but at different times. Inherently the temperature and pressure values at the beginning of the initial deployment are

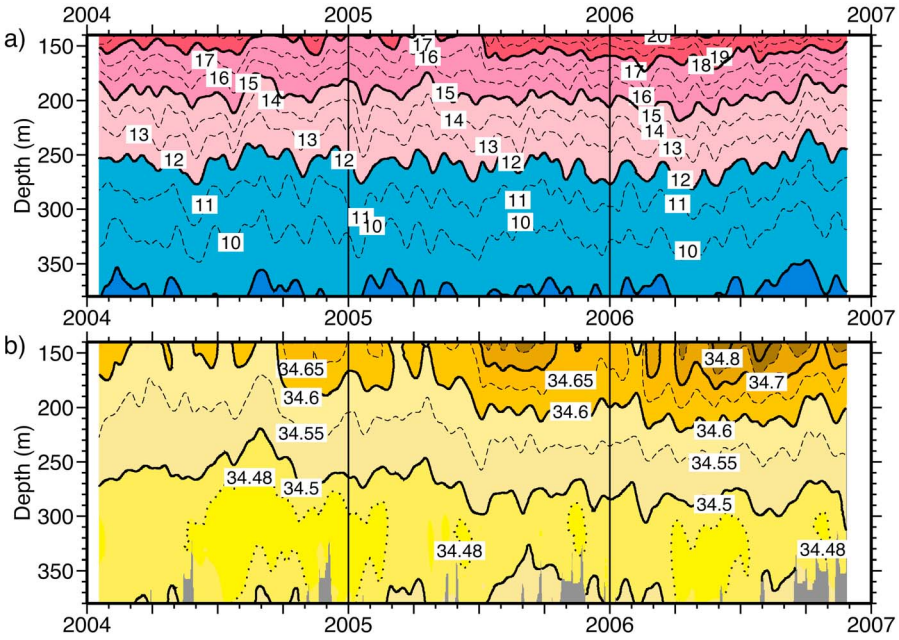

Figure 5. The Makassar Strait (a) temperature and (b) salinity time-sections constructed from the January 2004 through November 2006 INSTANT mooring observations. The temperature units are °C, and are considered accurate to within 0.1°C. The salinity units are in psu. Salinity values below ~250 m (i.e., below ~12°C), may be as much as 0.06 psu too salty, but the salinity changes over time and depth are thought to be generally accurate. The sections are filtered by 30 days.

most accurate, as, for example, the instruments are recently calibrated, are not yet compromised by any biologic growth on the sensors, and the maximum numbers of sensors are functioning. While the initial accuracy of the temperature sensors is reported to be ±0.002°C, to be conservative, we restrict our analysis to the assumption that that temperature data during the mooring deployment are valid to within 0.1°C.

[16] The combined INSTANT MAK-west and MAK-east temperature time series from 140 to 380 m is shown in Figure 5a. The relatively warmer water from late 2005 to 2006 (most obvious at shallower depths) defines a marked interannual feature. However, overall the temperature profile during the 3-year INSTANT program is much less variable then it was during the 1.5-year Arlindo program when there was the very strong 1997/1998 El Niño and significant shallowing of the isotherm depths midway into the measurement program [*Ffield et al.*, 2000]. During INSTANT the depth of the 30-day filtered 10°C isotherm varies only 61 m over 3 years (Table 1), but during Arlindo the depth of the 30-day filtered 10°C isotherm varies 264 m over just 1.5 years. Of course the isotherm depth variation values are all larger with less filtering; for example, with an hourly filter (not shown) – which retains tidal variability – the depth of the 10°C isotherm varies 204 m over the 3-year INSTANT time period.

[17] A combined MAK-west and MAK-east time series of salinity, with 6-minute time steps and nominal depths spanning between 115 and 294 m, was obtained from the four CTD instruments recovered from the 2004 to 2006 INSTANT moorings (Figure 5b). As noted above, the CTD instruments are swept downward by strong velocities, and then return to shallower levels when velocities weaken. However, there are only four CTD instruments, and conductivity, which is measured, and used with simultaneous measurements of temperature and pressure to calculate ocean salinity, is a more challenging parameter to determine than temperature alone. Additionally, as the Makassar thermocline has considerable heaving (tens of meters) at short time scales (minutes), it is difficult to adequately calibrate 3 years of salinity mooring values. Comparison with historical CTD cast data suggests that the salinity values below ~250 m (i.e., below ~12°C), may be as much as 0.06 psu too salty. The shallower mooring salinity values are within

Table 1. The 15° and 10°C Isotherm Depth Minimum, Maximum, and Range Revealing the Large Variability in the Makassar Strait Thermocline

	15°C Isotherm Depth			10°C Isotherm Depth		
	Range (m)	Minimum	Maximum	Range (m)	Minimum	Maximum
Arlindo (1997–1998.5), 30-day filter	82	186	268	264	282	546
INSTANT (2004, 2005, 2006), 30-day filter	47	173	220	61	290	351
INSTANT, hourly filter	125	141	266	204	230	434
INSTANT, hourly filter, first month	78	156	234	110	271	381

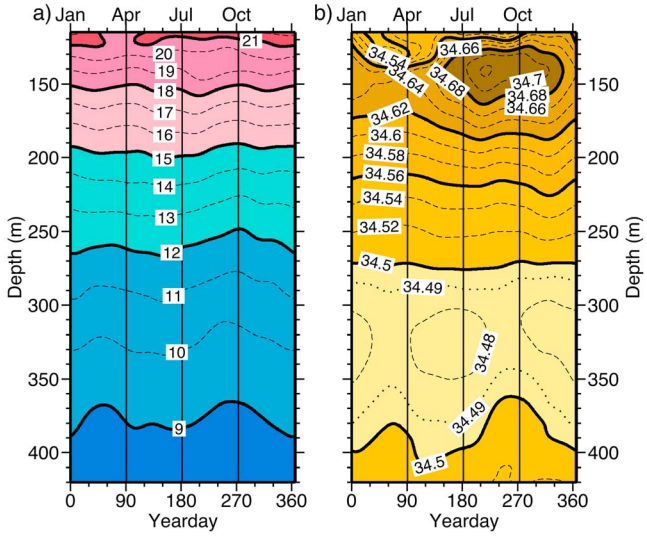

Figure 6. The Makassar Strait (a) temperature (°C) and (b) salinity (psu) mean seasonal sections constructed from the January 2004 to November 2006 INSTANT mooring measurements. In this figure, the depth axes are extended to 110 to 420 m, as the mean seasonal averaging of 3 years of data at each grid point enables smooth contouring even at the depth extremes where mooring blow over enables intermittent sampling. A 3-month low-pass filter has been applied before contouring.

the historical range, but a more definitive assessment of the salinity accuracy could not be made. It is quite evident that the salinity does change over time, which we consider oceanographically significant, as the changes provide time-evolution detail to snapshot ship-based studies. Therefore, in order to capitalize on the advantages of this particular data set, this analysis focuses on salinity changes, and not on absolute salinities. None-the-less, the measurements provide the first long-term salinity time series of the Makassar water column: It is evident that the warmer water observed from late 2005 to 2006 (Figure 5a), is coupled to a simultaneous trend toward saltier water (Figure 5b), indicative of a temporal change in the water masses.

[18] Temperature and salinity mean seasonal (Figure 6) and interannual anomaly (Figure 7) sections were constructed with the 3-year 2004–2006 INSTANT measurements, using the same filtering methodology described above for velocity. The INSTANT near-surface mean seasonal temperature and salinity signal (Figure 6) is similar to that observed in Arlindo, but now the salinity observations are well resolved in time: The warmest, freshest surface water occurs in the December through March period, and the coolest, saltiest surface water occurs in the June through November period [*Ilahude and Gordon*, 1996]. The low-salinity variability observed in the INSTANT near-surface layer (above the 34.54 psu contour in January–March at depths less than 135 m, Figure 6b) is possibly from the Java Sea as observed by *Fang et al.* [2010] in December 2007 to February 2008 in the Karimata Strait. During the northwest monsoon (January to March), low-salinity surface water from the Java Sea moves into the southern Makassar Strait, whereas during the southeast monsoon (July to September), the southeast monsoon winds return the low-salinity water into the Java Sea [*Gordon et al.*, 2003b]. The low-salinity Java Sea surface water is constrained to the upper ~50 m until it leaves the shallow Java Sea shelf. At slightly deeper levels, the salinity (and temperature) changes reflect the velocity variability in the Makassar subsurface velocity maximum core (derived from the Mindanao Current [*Gordon*, 2005]), with the highest salinities (greater than 34.7 psu near 140 m) from July–October (Figure 6b) directly corresponding to the highest velocities (greater than 0.7 m/s near 120 m) from July–September (Figure 3). Below 250 m, the mean seasonal

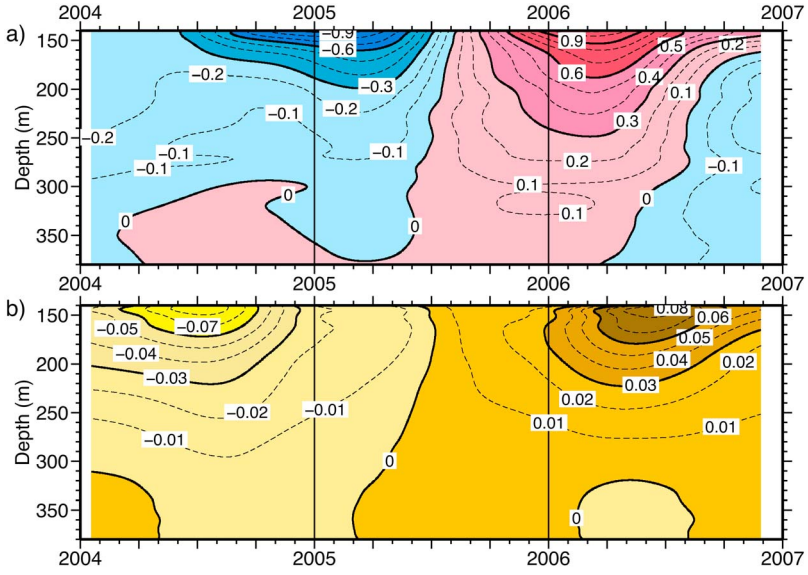

Figure 7. The Makassar Strait (a) temperature (b) salinity interannual anomaly time-sections constructed from the January 2004 to November 2006 INSTANT mooring measurements. A 6-month low-pass filter has been applied before contouring.

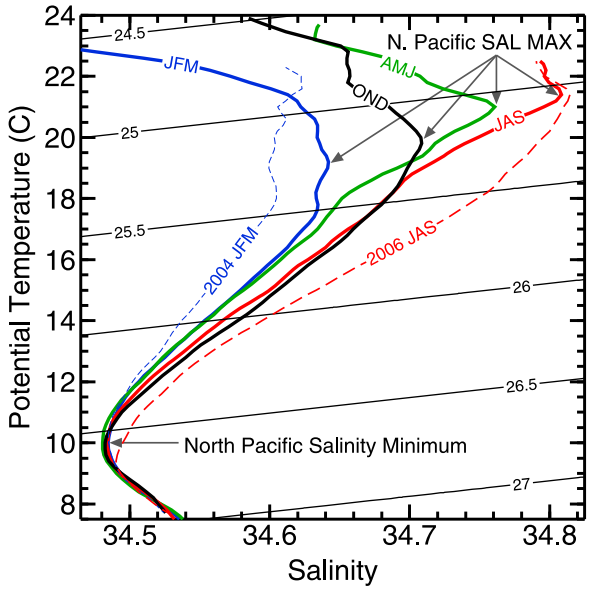

Figure 8. The Makassar Strait potential temperature-salinity curves constructed from the January 2004 to November 2006 INSTANT mooring measurements, restricted to data below 140 m. The four monsoon seasons are shown: January–February–March (JFM, blue), April–May–June (AMJ, green), July–August–September (JAS, red), October–November–December (OND, black), and the two most-contrasting monsoon occurrences: 2004 northwest monsoon ("2004 JFM," blue dashed) and 2006 southeast monsoon ("2006 JAS," red dashed). The North Pacific salinity maximum ("N Pacific SAL MAX," ~140 m depths) and the "North Pacific Salinity Minimum" (~320 m depths) are indicated by black arrows. Note that the INSTANT temperature and salinity data set does not include surface values, which would be the warmest (and typically the freshest) values of the Makassar water column.

temperature and salinity values seem to indicate variability associated with the semi-annual northward intrusion of Kelvin waves; for example, at 400 m the deeper isotherms and isohalines in May–June and in November–December (Figure 6) correspond to the May and November Kelvin wave reduced southward velocities (Figure 3).

[19] Despite the less variable INSTANT temperature profiles (as compared to Arlindo 1996–1998), there are significant interannual anomaly temperature changes (Figure 7a) throughout the thermocline during 2004–2006: anomaly temperatures are cooler then −0.8°C at 140 m (e.g., a shallowing of the isotherms) at the end of 2004 and beginning of 2005 consistent with El Niño conditions, and anomaly temperatures are warmer then 1.0°C at 140 m (e.g., a deepening of the isotherms) in the beginning of 2006 consistent with La Niña conditions. Previous studies have shown that the average Makassar temperature is highly correlated to ENSO [*Ffield et al.*, 2000]. With this data set, the 3-month filtered, average 120–420 m Makassar temperature is also consistent with a high correlation to ENSO, with r = −0.78 for NINO3.4. It is important to note that even if the Makassar velocities are not impacted by ENSO at any point in time, the Makassar velocities will still carry ENSO-impacted Makassar temperature changes from the Mindanao Current through the Makassar Strait, bolstering the relationship of the Makassar temperatures to ENSO and potentially impacting regional sea surface temperatures and climate.

[20] The INSTANT salinity profiles also reveal interannual anomaly salinity changes (Figure 7b): anomaly salinities are shown as fresher than −0.07 at 140 m in the middle of 2004, and as saltier than 0.07 psu at 150 m in the middle of 2006. However, this first long-term salinity time series of the Makassar water column is not consistent with a high correlation to the ENSO indices (r = −0.09 for NINO3.4 with the 3-month filtered, average 120–420 m salinity). This result can be discerned visually by examining Figure 7 near 150 m, where at first glance the interannual variability in temperature and salinity seem similar because they both change phase in mid-2005, but in fact the predominate temperature minimum and maximum signals are separated by ~12 months, whereas the predominate salinity minimum and maximum signals are separated by ~23 months. Instead, the observed interannual salinity signal seems to be consistent with ENSO induced changes in the South China Sea throughflow, as revealed by the HYCOM model and described in *Gordon et al.* [2012]: low-salinity surface water from the Sulu Sea accumulates in the western Sulawesi Sea and northern Makassar Strait during prolonged El Niño conditions (specifically during the 2004 El Niño period), with the gradual return of saltier upper layer water from the equatorial North Pacific during La Niña conditions. The implication is that the accumulation of low-salinity surface water and the gradual return of saltier upper layer water, while indirectly induced by ENSO, are not in lock step with Pacific ENSO timing. Further south along the ITF throughflow route, at the INSTANT moorings, vertical mixing will have spread a diluted form of these upper layer salinity signals down deeper into the water column, possibly explaining the INSTANT observations of low-salinity interannual anomalies evident down to ~250 m in 2004, and high-salinity interannual anomalies evident down to ~250 m in 2006 (Figure 7b). The potential significance relates to the importance of accurately identifying the source and modification of the water properties carried by the ITF into the Indian Ocean.

[21] The vertical placement of the conductivity sensors on the INSTANT moorings was designed to capture the variability in the shallow North Pacific subtropical salinity maximum and the deeper North Pacific subpolar salinity minimum [*Ilahude and Gordon*, 1996], the two key water mass features within the Makassar thermocline, whose eventually destruction within the Indonesian seas is indicative of mixing processes [*Ffield and Gordon*, 1992]. These two features are best identified in a potential temperature–salinity plot (Figure 8), as it is the linkage of temperature and salinity to each other that defines water mass features. The highest salinities within the upper thermocline, generally at 140 m depth, reveal the core of the inflow of North Pacific salinity maximum water (Figure 8, black arrows). The signal is strongest in July–August–September (JAS), and in particular during JAS 2006, directly associated to the time and depth intervals with the highest southward velocities (Figures 3 and 4). The high velocities presumably inject more North Pacific salinity maximum water through the Makassar Strait, enabling a concentrated salinity maximum feature to survive further down into the Makassar Strait. The signal is weakest or most eroded by vertical mixing, in

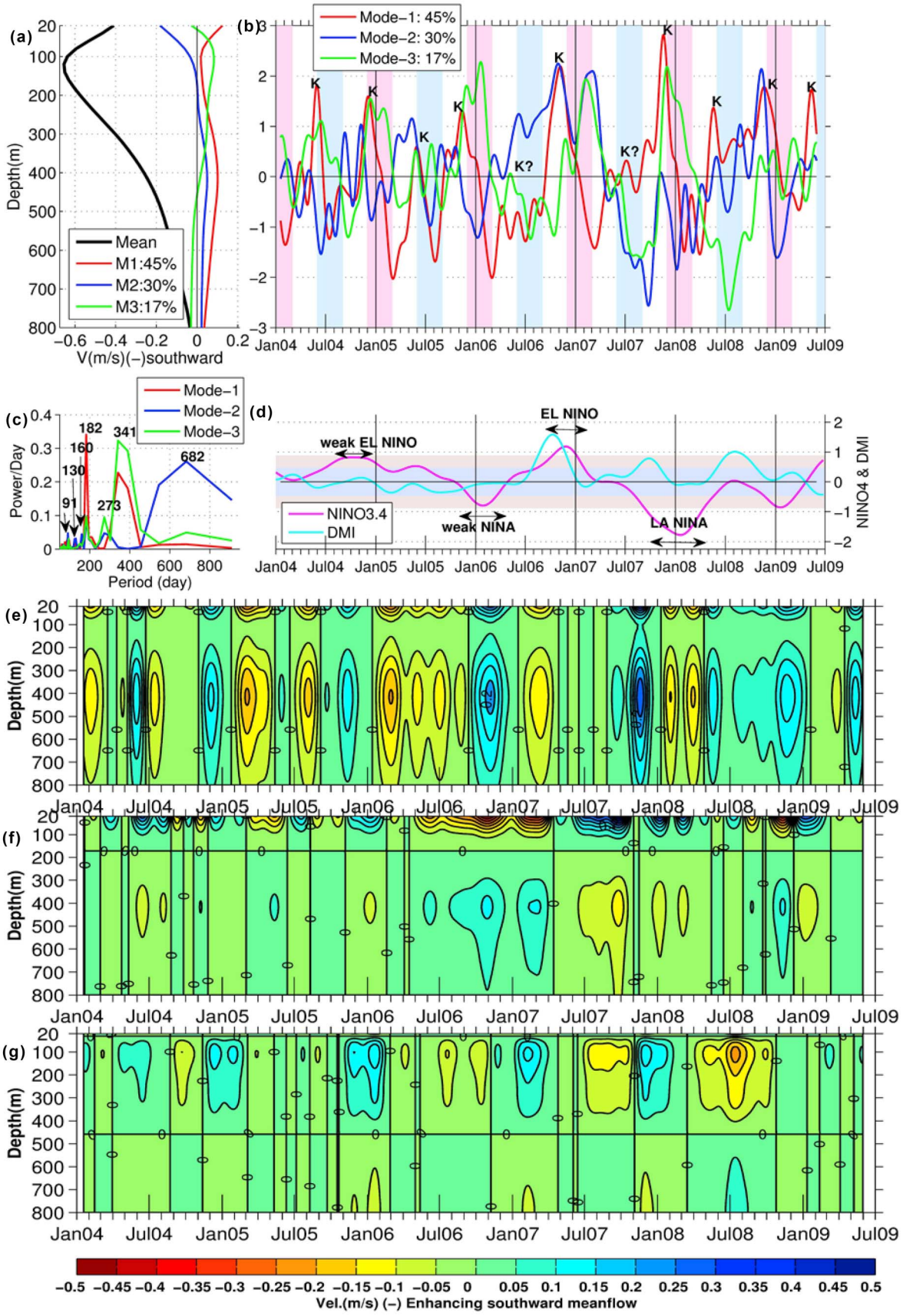
(a)
Depth(m)
Mean
M1:45%
M2:30%
M3:17%
V(m/s)(−)southward
(b)
Mode−1: 45%
Mode−2: 30%
Mode−3: 17%
K
K?
(c)
Power/Day
Mode−1
Mode−2
Mode−3
182
160
130
91
341
273
682
Period (day)
(d)
EL NINO
weak EL NINO
weak NINA
LA NINA
NINO3.4
DMI
NINO4 & DMI
(e)
(f)
(g)
Depth(m)
Jan04 Jul04 Jan05 Jul05 Jan06 Jul06 Jan07 Jul07 Jan08 Jul08 Jan09 Jul09
−0.5 −0.45 −0.4 −0.35 −0.3 −0.25 −0.2 −0.15 −0.1 −0.05 0 0.05 0.1 0.15 0.2 0.25 0.3 0.35 0.4 0.45 0.5
Vel.(m/s) (−) Enhancing southward meanflow

Figure 9

January–February–March (JFM), and in particular during JFM 2004, associated with low salinities at the near-surface (possible Java and Sulu Sea inputs) and weak southward velocities. The water mass analysis also reveals that, as expected, there are no indications of any South Pacific water within the Makassar Strait; although, theoretically this remains a possibility, as upstream in the equatorial Pacific there have been occasional observations of South Pacific water just offshore of the Mindanao Current [e.g., *Wijffels et al.*, 1995] that possibly could be incorporated into the Makassar Strait source waters.

4. Vertical Mode Structure and Its Temporal Variability

[22] Empirical Orthogonal Function (EOF) analysis is used to investigate the mode structure of the velocity profile time series and its temporal variability. The temporal mean velocity below 750 m is less than 0.02 m/s, indicating that the bulk of the throughflow, as reported earlier, occurs above the Makassar sill depth, of approximately 680 m [*Gordon et al.*, 2003a]. As most of the throughflow resides in the upper 750 m (both MAK-west and MAK-east moorings have a current meter at the nominal depth of 750 m) the EOF analysis of the integrated velocity profile is only performed for the upper 800 m. Before applying the EOF analysis, the temporal mean velocity profile (solid black line in Figure 9a; the 2004–2009 mean full-depth throughflow is consistently directed southward) has been removed. The surface velocity of the mean flow is −0.4 m/s, with a maximum flow of −0.7 m/s at 120 m. The temporal mean velocity profile represents the large-scale pressure gradient between the Pacific and Indian Oceans that drives the ITF [*Wyrtki*, 1987].

[23] The EOF analysis gives the vertical mode structures (Figure 9a; red, blue, and green lines) and their normalized temporal mode variability relative to the mean flow (Figure 9b; red, blue, and green lines). Normalized temporal variability shows the time-varying element of the vertical mode structure, which enables us to calculate the velocity variability relative to the mean flow (Figures 9e–9g) by multiplying the vertical mode structures (Figure 9a) and the temporal variability (Figure 9b). To determine the direction of the mode velocities relative to the southward mean flow, the sign of the vertical mode structure must be multiplied by the sign of the temporal mode variability. Negative values denote southward, or enhancing the southward mean flow, while positive values denote northward, or reducing the southward mean flow (Figures 9e–9g).

[24] The EOF analysis reveals that the first three dominant modes account for 92% of the total variance, with the first, second, and third mode accounting for 45%, 30%, and 17% of the variance, respectively.

4.1. Mode 1: Indian Ocean Kelvin Waves

[25] The first mode (Figure 9a, red line) accounting for 45% of variance is characterized by low vertical shear (relative to the baroclinic mean; Figure 9a, black line). The vertical structure shows a gradual decay from the maximum at the surface to around 100 m and a gradual increase at 400 m and a gradual decay below this depth. Frequency analysis of the first mode reveals peaks at semiannual and annual periods (Figure 9c). Given the complex nature of the coastline geometry and bathymetry, as well as the atmospheric-oceanic forcing affecting the dynamics of the Indonesian seas, it is a challenge to separate the Kelvin waves from the monsoon forcing in the EOF modes. Therefore, we not only need to use the vertical structure of the EOF modes (Figure 9a), but also their temporal variability (timing, Figure 9b), spectral analysis (Figure 9c), and a combination of vertical structure and temporal variability (Figures 9e–9g) to distinguish the signals. Based on the timing of the events, the strong negative values of the first mode temporal variability, i.e., northward flow anomaly at the end of May and November (Figure 2a), are associated with the intrusions of semiannual coastally trapped Kelvin waves from the Indian Ocean (Figure 9b marked by "K"; Figure 9e) [i.e., *Arief and Murray*, 1996; *Iskandar et al.*, 2005; *Potemra et al.*, 2002; *Sprintall et al.*, 2000] forced by the semiannual Wyrtki Jet in the equatorial Indian Ocean [*Nagura and McPhaden*, 2010; *Qiu et al.*, 2009; *Wyrtki*, 1973]. These coastally trapped Kelvin waves propagate eastward along the equatorial Indian Ocean and along the western coast of Sumatra and southern Java and partially enter the Lombok Strait. While small wind fluctuations occur year-round over the equatorial Indian Ocean inducing Kelvin Waves that impinge on Lombok and Ombai Straits [*Drushka et al.*, 2010; *Arief and Murray*, 1996; *Hautala et al.*, 2001; *Potemra et al.*, 2002], it is the major wind perturbations of the monsoonal transition seasons that produce strong, semi-annual Kelvin Waves, or Wyrtki Jets, that clearly reach into and alter the Makassar Strait throughflow in May and November [*Sprintall et al.*, 2000; *Susanto et al.*, 2000]. Recently, numerical models simulated the intrusion of Kelvin waves from the Indian Ocean into the Makassar Strait [*Shinoda et al.*, 2012].

[26] The correlation between the first mode time series and the velocity at deeper layers (Figure 10a) is higher than that at upper layers, and the mean seasonal velocity contours tilt right (delayed as depth shoals) in Figure 3 following the cores of the lowest velocities from 800 m to 180 m associated with the semi-annual Kelvin waves in May and November, indicating that Kelvin waves are characterized

Figure 9. Empirical Orthogonal Function (EOF) of the Makassar Strait velocity (m/s). (a) The time series profile mean (black), and the vertical mode structure of mode 1 (red), mode 2 (blue) and mode 3 (green). (b) The normalized temporal variability of the velocity structure time series, modes 1, 2, 3, which together account for 92% of the total variance. Semi-annual Kelvin wave intrusions are marked by "K." Season grouping is assumed 1-month delay from the monsoonal winds. Peak of southeast monsoon is shaded in cyan, while peak of northwest monsoon is shaded in magenta. (c) Spectral estimates of the EOF modes. (d) Time series of NINO3.4 index (red) and DMI (cyan). Standard deviation of NINO3.4 (shaded magenta) and DMI (shaded cyan). (e) Velocity variability relative to the mean flow for the (e) first, (f) second and (g) third modes. Negative values denote southward, or enhancing the southward mean flow, while positive values denote northward, or reducing the southward mean flow.

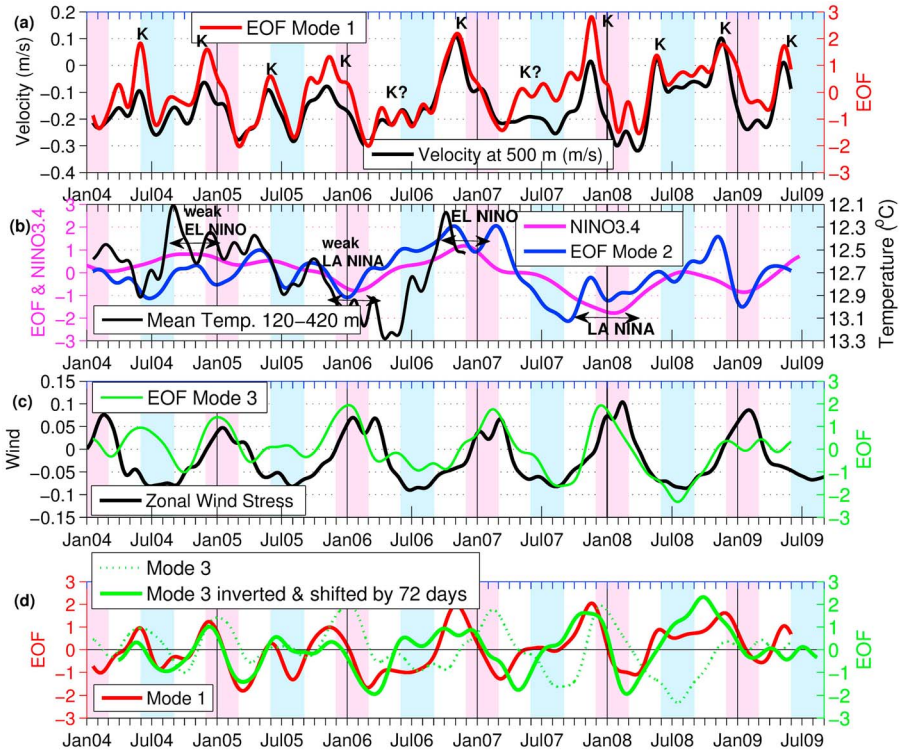

Figure 10. (a) Velocity at 500 m and EOF mode 1 with correlation value (r = +0.87) between the two. Mode 1 is associated with semiannual Kelvin waves from the Indian Ocean. The intrusions of Kelvin waves ("K") reduce the mean southward Makassar Strait velocity. There are no apparent propagations of Kelvin waves in May prior to the El Niño 2006/2007 and the La Niña 2007/2008. (b) NINO3.4 (magenta) and the second mode time series (blue) and the average temperature between 150 and 450 m (black). The correlation between the second mode and NINO3.4 is r = 0.6 after advancing the second mode by 3 weeks. (c) The third mode time series (green) and the monsoon winds (black). (d) The first (red) and third (dotted green) mode time series. The correlation between the two time series is r = −0.7 and the signal occurs 72 days earlier in mode 3. In order to more easily perceive the correlation, the third mode time series is also plotted inverted and shifted later in time by 72 days (solid green); note that none of the plot axes correspond to this inverted and shifted time series.

by upward propagating phase or downward energy propagation [*Drushka et al.*, 2010]. The correlation value between the Makassar velocity at 500 m and mode 1 is r = +0.87 (Figure 10a). En route to the Makassar Strait, it is possible that Kelvin waves may be altered by time/distance/sill-depths from the forcing origin or by other dynamical processes, therefore it is unlikely that each of our modes only represents one pure signal. EOFs represent vertically standing waves relative to the mean throughflow. Hence, mode 1 represents an average vertical structure of Kelvin waves and their temporal variability. Detailed results of the upward propagation phases and their variability are beyond scope of the paper and will be presented in a future manuscript. The intrusion of the semi-annual Kelvin waves reduces the southward mean flow in the Makassar Strait and enhances the vertical shear velocity within the thermocline.

[27] The intensity of the coastally trapped Kelvin waves in May and November may be related to larger interannual forcing associated with ENSO and IOD phases. There are no clear Kelvin wave intrusions in the Makassar Strait in May prior to the 2006/2007 El Niño and in May prior to the 2007/2008 La Niña. The Wyrtki Jet was not clearly seen in either the observations or the numerical model during boreal fall 2006 [*Nagura and McPhaden*, 2010; *Vinayachandran et al.*, 2007]. However, during the peak of El Niño in late 2006 when NINO3.4 and Dipole Mode Index (DMI) are both strongly positive (Figure 9d), the Kelvin wave intrusion in November is stronger, being strongest in the 2007/2008 La Niña when DMI is nearly zero. A similar pattern is observed in the Arlindo data during the strong 1997/1998 El Niño and a strong positive DMI as well as a strong Kelvin wave intrusion into the Makassar Strait [*Sprintall et al.*, 2000; *Susanto and Gordon*, 2005]. Moreover, during the La Niña condition in 1998 (negative NINO3.4), there was no clear evidence of a Kelvin wave intrusion in May 1998 [*Susanto and Gordon*, 2005]. During the development of El Niño with positive DMI (April–May), strong anomalously easterly winds occur along the southern coasts of Java and Sumatra and in the equatorial Indian Ocean causing strong upwelling and a shoaling thermocline, and lower sea level and sea surface temperature [*Susanto et al.*, 2001; *Webster et al.*, 1999]. These anomalies in wind events may excite weak upwelling Kelvin waves in the equatorial Indian Ocean, which may not be able to reach the Makassar Strait. During the development of La Niña, westerly winds in the Indian Ocean are weak which may generate weak downwelling

Kelvin waves. Deeper thermoclines in the western tropical Pacific Ocean and eastern tropical Indian Ocean may inhibit the intrusion of Kelvin waves through the Lombok Strait, possibly explaining the lack of a Kelvin wave intrusion in May/June 2007.

4.2. Mode 2: ENSO Modulation of Rossby Waves From the Pacific Ocean

[28] The second mode (Figure 9a, blue line) accounting for 30% of the variance is characterized by a vertical structure with opposing flow separated at 200 m, and with a surface intensification which is resembles a second baroclinic dynamical mode [*Wajsowicz et al.*, 2003]. The second mode variability in depth and time is shown in Figure 9f. The temporal variability is associated with the ENSO modulation (Figure 10b) of Rossby waves from the Pacific Ocean with periods less than a year [*Cravatte et al.*, 2004; *Qiu et al.*, 1999]. Because of a "leaky" western Pacific boundary, westward propagating Rossby waves in the Pacific may be able to enter the Sulawesi Sea [*Boulanger et al.*, 2003]. Spectral analysis of the temporal variability of the second mode reveals peaks at 91, 120 and 160 days (Figure 9c, blue line). The intraseasonal (<90-day period) waves are probably the same as reported by *Pujiana et al.* [2009] in their analysis of the velocity data focusing on 20- to 100-day wave periods.

[29] Recently, *Kashino et al.* [2011] reported semiannual, annual and interannual features observed on their TRITON moorings, which are associated with westward propagating Rossby waves and ENSO. Similar features are also reported by *Qu et al.* [2008] based on sea level anomaly data. Though longer time series are needed, a correlation (r = 0.6) between the second mode time series and the NINO3.4 index indicates an ENSO modulation on the Rossby waves (Figure 10b). The second mode precedes the NINO3.4 index by 3 weeks. The lead time may represent the time difference between the ENSO signal to impact velocities in the Makassar Strait (the western Pacific boundary is always open allowing Pacific water flow into the Makassar Strait), and the equatorial Pacific Kelvin waves (average speed of 2.5 m/s) [*Susanto et al.*, 1998] to carry warm water from the western Pacific into the NINO3.4 region. Interannual variability of the ITF has been linked to ENSO [i.e., *England and Huang*, 2005; *Meyers*, 1996]. As described above, the average temperature between 120 and 420 m (Figure 10b) is consistent with a high correlation to ENSO (r = −0.78 with NINO3.4), such that cooler water is observed in the Makassar Strait during El Niño (shallower isotherms) and warmer water during La Niña (deeper isotherms). However, in regard to the heat transport actually carried by the ITF, the effect of the ENSO velocity profile changes mitigate the ENSO temperature changes, because when the Makassar thermocline is cooler (warmer) during El Niño (La Niña), the southward Makassar velocities are enhanced (reduced) in the warm surface layer and reduced (enhanced) in the cool deeper layers resulting in a counteracting warming (cooling) component to the transport-weighted temperature carried by the ITF.

4.3. Mode 3: Regional Monsoon Winds

[30] The third mode (Figures 9a and 9b, green line), accounting for 17% of the total variance and resembling the third baroclinic dynamical mode [*Wajsowicz et al.*, 2003], is associated with regional monsoon winds. The third mode is characterized by a three-layer flow with two zero crossings at 50 m and 450 m with a sub-surface/thermocline intensification with maximum at 100 m (Figure 9a, green line; Figures 9e–9g). Figure 9g shows the third mode velocity variability in depth and time. Hence, the monsoon winds mostly affect the Makassar velocity at 100 m depth. The second and third mode structures of the observed Makassar velocity profile are similar to the first and second modes generated by a numerical model [*Potemra et al.*, 2003]; however, there is no mode in the model that looks like mode 1 reported here, which is probably because the model resolution does not allow Kelvin waves to enter the Lombok Strait, i.e., the Strait was closed.

[31] Based on the spectral analysis there are many peaks, which indicate multiple forcing mechanisms, with the strongest peak at 341 days associated with the regional monsoon winds. During the boreal winter (December to March) the South China Sea throughflow via Karimata Strait is strong [*Fang et al.*, 2005, 2010; *Susanto et al.*, 2010] where monsoon winds drive low salinity, buoyant water from the South China Sea-Java Sea into Makassar Strait reducing the southward mean Makassar throughflow [*Gordon et al.*, 2003b], while during the summer monsoon (June–August) the monsoon winds tend to enhance southward mean throughflow. Figure 10c shows the third mode time series and the average of the regional monsoon wind stress in the Indian Ocean and Java Sea (12°S to 3°S and 109°E to 120°E). The daily gridded (0.5° × 0.5° resolution grids) QuikSCAT winds are obtained from http://cersat.ifremer.fr/.

[32] Interestingly, there is also a high correlation (r = −0.7) between the first (red) and the third mode time series (dotted green; Figure 10d) and the signal occurs 72 days earlier in mode 3. In order to more easily perceive the correlation, the third mode time series is also plotted inverted and shifted later in time by 72 days (solid green; Figure 10d). Both modes follow an annual/semiannual cycle forced by the regional monsoon winds, but with slightly different timings. During the monsoon transitions in April–May and October–November, the wind variability in the Indian Ocean induces a Wyrtki Jet and generates eastward propagation of coastal Kelvin waves (captured as EOF mode 1). Meanwhile, during the peak of the monsoon winds in the boreal winter (summer), the Makassar throughflow is reduced (enhanced) as captured by EOF mode 3.

5. Transport Variability

[33] The nearly 5.5 year record of Makassar velocity profile is used to estimate the full-depth Makassar volume transport, the largest transport component of the total ITF [*Gordon*, 2005]. The two INSTANT moorings are 19.4 km apart within the 45 km wide Labani channel for the period 2004–2006, with only the western mooring continued for the period 29 November 2006 to 31 May 2009. The calculation of the Makassar Strait throughflow requires a methodology to determine the full transport passing between the western and eastern sidewalls (Figure 1). Following a similar approach as *Sprintall et al.* [2009] for the ITF Sunda passages, three schemes with 1-km-wide and 10-m-thick bins, were chosen for across-strait interpolation between the moorings and for extrapolation to the sidewalls for the

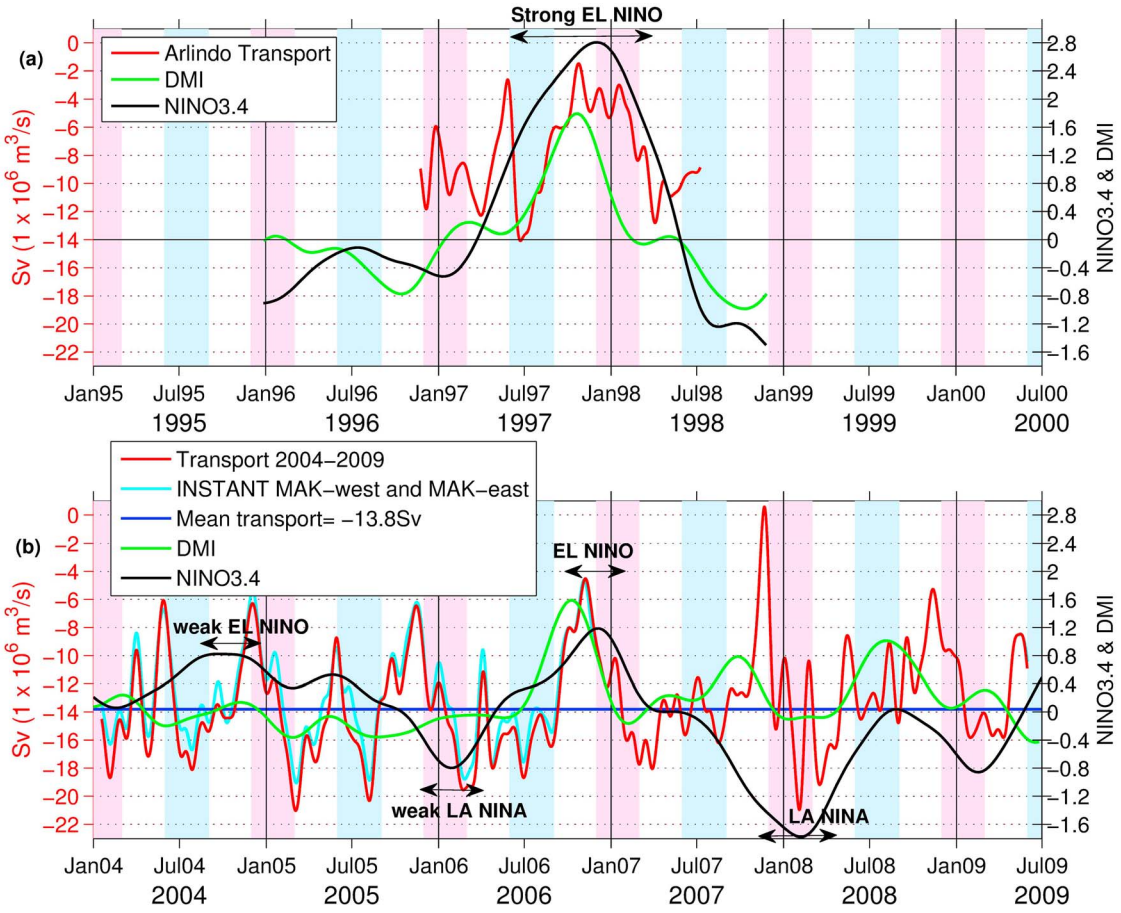

Figure 11. The Makassar Strait volume transport time series (Sv; red) and overlaid with NINO3.4 and IOD indices. (a) During the period of Arlindo program 1996–1998 and (b) during and post INSTANT program from 2004 to 2009 with an annual mean of −13.3 Sv. For comparison, an estimate of Makassar Strait transport during the INSTANT program 2004–2006 derived from combined MAK-west and MAK-east data (Sv, cyan), which is slightly lower (3-years mean = −12.8 Sv) than that of MAK-west data only (3-year mean = −13.8 Sv). For clarity, a monthly low-pass filter has been applied to the transport time series. The peak of the southeast monsoon is shaded in cyan, while the peak of northwest monsoon is shaded in magenta. The seasonal grouping is delayed 1 month from the monsoonal winds.

2004–2006 period: (1) "mean": averaged velocity of MAK-west and MAK-east uniformly extrapolated across the total width of the strait (this is the scheme used by *Gordon et al.* [2008]); (2) "block": evenly dividing the across-strait distance between the moorings and assigning the MAK-west velocity for the western side and the MAK-east velocity for the eastern side; and (3) "linear": extrapolating a linear fit between the moorings to the sidewalls.

[34] Given the short north–south length (25 km) of the Labani Channel and that the moorings are situated within 10 km of the northern entrance to the channel, with characteristic southward speeds of 0.1 to 0.7 m/sec, we assumed that the sidewall boundary layer is not yet fully developed and can be considered to be very narrow. Therefore, as in *Sprintall et al.* [2009], in all schemes, zero flow is assumed in the 1-km bins adjacent to the sidewalls. Our western boundary neglects the broad shallow region to the west of the Labani Channel that is fringed by many coral reefs and small islands.

[35] All three schemes give a similar total volume transport for the Makassar Strait. The 2004–2006 3-year average transports for the mean, block, and linear schemes are −12.6 Sv, −12.7 Sv, and −12.9 Sv, respectively. This value is slightly higher than initially estimated (−11.6 Sv [*Gordon et al.*, 2008]). The difference is due to the utilization of finer bathymetry data in the upper 750 m that was obtained during field work in 2009. The 3-year average gives nearly identical total volume transports, with the differences between the schemes less than 0.3 Sv, which indicates that the Makassar Strait transport estimates are not overly sensitive to the choice of interpolation/extrapolation schemes. The ∼1 Sv increase of the 3-year INSTANT period Makassar transport derived with the improved bathymetry, reduces the ITF inflow/outflow imbalance reported by *Gordon et al.* [2010] from 2.3 Sv to 1.3 Sv.

[36] The ensemble average of these three schemes transport estimates is shown in Figure 11b (cyan color), while the average transport calculated based solely on the MAK-west

mooring for the entire period 2004–2009 is shown Figure 11b (red line). For comparison, the 2004–2006 mean transport based solely on MAK-west is −13.8 Sv with a standard deviation of 3.7 Sv. Whereas the 2004–2006 mean of the ensemble transport of MAK-west and MAK-east is −12.8 Sv and a standard deviation of 3.3 Sv. This result indicates that Makassar transport derived from a single mooring deployed at the MAK-west site will over-estimate the transport by ∼1.0 Sv.

[37] There is clear consistency in the annual average transport. The Makassar volume transport is southward throughout the record, interrupted only during strong, semi-annual Kevin wave events (e.g., November 2007). The annual mean transport from 2004 to 2009 is −13.3 Sv with a standard deviation of 3.6 Sv (Sv = 10^6 m^3/s), displaying small year-to-year variability: −13.4 Sv, −14.0 Sv, −13.8 Sv, −13.1 Sv, −12.5 Sv, −13.1 Sv for 2004 to 2009, respectively. Assuming that the MAK-west and MAK-east velocity ratio holds for 2007–2009 period, our 2007–2009 annual transport estimates may be 1.0 Sv too high. The transport results support the previous conclusion that there is a substantial increase (about 38%) in the annual mean transport observed during the 2004–2006 INSTANT period relative to that observed during the 1996–1998 Arlindo program when the strong 1997/1998 El Niño reduced the southward flow (Figure 10a; −9.1 Sv in *Gordon et al.* [1999] and −9.2 Sv in *Susanto and Gordon* [2005]). In contrast to the strong El Niño during the Arlindo program, during the 2004–2009 period, the ENSO phase was in a relatively neutral state with the relatively weak 2006/2007 El Niño with a positive DMI and the relatively weak 2007/2008 La Niña with a neutral DMI.

[38] The Makassar Strait transport displays both seasonal and interannual variability. In the upper layer and thermocline (0–230 m), the maximum transport occurs during the peak summer/southeast monsoon (June–August). Conditions are reversed in the lower thermocline and in the deeper layer where the maximum transport occurs during the peak of the northwest monsoon (January–March). The minimum transport for the entire water column occurs during the monsoon transition in October to December. The seasonal averaged transports are −15.5 Sv, −13.7 Sv, −14.2 Sv, and −9.6 Sv for the northwest monsoon (JFM), first monsoon transition (AMJ), southeast monsoon (JAS), and second monsoon transition (OND), respectively.

[39] The Makassar Strait transport reveals interannual variability, with the lowest transport (+0.6 Sv) in November 2007 during the strong intrusion of the Kelvin wave just prior to the 2007/2008 La Niña when the DMI is positive (Figure 11). This condition lasted for 1 week only. The second lowest transport (−4.5 Sv) was during the 2006/2007 El Niño when the DMI is positive. The strongest southward transport (−21.0 Sv) occurs in January 2005 and in February 2008, during a mature 2007/2008 La Niña when IOD is neutral.

6. Summary

[40] The mean and variability of velocity, temperature, salinity, and associated volume transport of the ITF within the Makassar Strait are determined. The Makassar Strait throughflow is thermocline intensified and highly variable across a broad range of frequencies from tidal, intraseasonal, seasonal to interannual time scales. The 2004–2009 seasonal mean velocity clearly reveals maximum southward velocity in July to September during the southeast monsoon, and exhibits semi-annual Kelvin waves from the south in May and November. As previously observed, the Makassar temperature variability is highly correlated to ENSO. In contrast, the first measurements of salinity at these time-scales and depths reveal that the salinity variability is not directly correlated to ENSO. The salinity variability does reveal possible Java Seawater input from the south at monsoon time-scales and possible Sulu Seawater input from the north at interannual time-scales.

[41] The mean velocity profile in the Makassar Strait is controlled by the large scale pressure gradient between the Pacific and Indian Oceans, while the variability is controlled by the equatorial winds in the Indian Ocean that induce Kelvin waves, and the equatorial winds in the Pacific Ocean that cause westward propagating Rossby waves and ENSO. The Kelvin waves enter the Makassar Strait from the south, in opposition to the Rossby waves entering the Makassar Strait from the north, complicating the observed velocity variability. The EOF analysis of the 2004–2009 Makassar velocities separates the signals with the first three dominant modes accounting for 92% of the total variance. The first mode is associated with northward intrusions of semiannual Kelvin waves from the Indian Ocean. The second and third vertical EOF mode structures resemble the second and third baroclinic dynamical modes shown by *Wajsowicz et al.* [2003]. The second mode is probably associated with Rossby waves from the Pacific Ocean with periods less than a year and modulated by the ENSO phase [*Cravatte et al.*, 2004]. The third mode is associated with the regional monsoon winds: during the boreal winter monsoon the winds reduce the Makassar throughflow, while during the boreal summer monsoon the winds enhance the throughflow.

[42] Even though the transport is closely related to the ENSO phase with stronger southward transport during La Niña and lower transport during El Niño [*Ffield et al.*, 2000; *Gordon et al.*, 1999; *Susanto and Gordon*, 2005] the strength of the northward intrusions of the Kelvin waves plays an important role in the total transport. The 2004–2009 annual mean transport is −13.3 Sv, with a standard deviation of 3.6 Sv, and with clear consistency of small year-to-year variability ranging from −12.5 Sv to −14.0 Sv. Therefore −13.3 Sv may serve as an annual climatic mean. Even though the annual mean variability is small, the transport variability is large, with the lowest transport of +0.6 Sv in November 18–24, 2007 during the strong intrusion of the Kelvin wave just prior to the 2007/2008 La Niña when the DMI is positive, and the strongest southward transport of −21.0 Sv occurs in January 2005 and February 2008, during a mature 2007/2008 La Niña when DMI is neutral. Future work includes detailing the forcing mechanisms and propagation of Kelvin wave intrusions and their impact on the transport in the Makassar Strait.

[43] **Acknowledgments.** The INSTANT data analysis is funded by the National Science Foundation (NSF) grants OCE-07-25935 (LDEO) and OCE-07-25561 (ESR). The time series analysis is partly supported by NSF grant OCE-07-51927. This research was funded in part under the Cooperative Institute for Climate Applications Research (CICAR) award number NA08OAR4320754 from the National Oceanic and Atmospheric

Administration, U.S. Department of Commerce. The statements, findings, conclusions, and recommendations are those of the authors and do not necessarily reflect the views of the National Oceanic and Atmospheric Administration or the Department of Commerce. We are grateful to our colleagues Indroyono Soesilo, Sugiarta Wirasantosa, Budi Sulistyo, and Irsan Brodjonegoro at the Agency for Marine and Fisheries Research (BRKP), Indonesia for their support of the INSTANT and MITF programs. Professionalism and support of the R/V *Baruna Jaya* and *Geomarin* officers and crews are appreciated. The Lamont-Doherty Earth Observatory contribution is 7576.

References

Aldrian, E., and R. D. Susanto (2003), Identification of three dominant rainfall regions within Indonesia and their relationship to sea surface temperature, *Int. J. Climatol.*, *23*(12), 1435–1452, doi:10.1002/joc.950.

Arief, D., and S. Murray (1996), Low-frequency fluctuations in the Indonesian throughflow through Lombok Strait, *J. Geophys. Res.*, *101*, 12,455–12,464, doi:10.1029/96JC00051.

Boulanger, J.-P., S. Cravatte, and C. Menkes (2003), Reflected and locally wind-forced interannual equatorial Kelvin waves in the western Pacific Ocean, *J. Geophys. Res.*, *108*(C10), 3311, doi:10.1029/2002JC001760.

Cravatte, S., J.-P. Boulanger, and J. Picant (2004), Reflection of intraseasonal equatorial Rossby waves at the western boundary of the Pacific Ocean, *Geophys. Res. Lett.*, *31*, L10301, doi:10.1029/2004GL019679.

Drushka, K., J. Sprintall, S. T. Gille, and I. Brodjonegoro (2010), Vertical structure of Kelvin waves in the Indonesian throughflow exit passages, *J. Phys. Oceanogr.*, *40*, 1965–1987, doi:10.1175/2010JPO4380.1.

Duchon, C. (1979), Lanczos filtering in one and two dimensions, *J. Appl. Meteorol.*, *18*, 1016–1022, doi:10.1175/1520-0450(1979)018<1016:LFIOAT>2.0.CO;2.

England, M., and F. Huang (2005), On the interannual variability of the Indonesian throughflow and its linkage with ENSO, *J. Clim.*, *18*, 1435–1444, doi:10.1175/JCLI3322.1.

Fang, G., R. D. Susanto, I. Soesilo, Q. Zheng, F. Qiao, and W. Zexun (2005), A note on the South China Sea shallow interocean circulation, *Adv. Atmos. Sci.*, *22*, 946–954, doi:10.1007/BF02918693.

Fang, G., Y. Wang, Z. Wei, Y. Fang, F. Qiao, and X. Hu (2009), Interocean circulation and heat and freshwater budgets of the South China Sea based on a numerical model, *Dyn. Atmos. Oceans*, *47*, 55–72, doi:10.1016/j.dynatmoce.2008.09.003.

Fang, G., R. D. Susanto, S. Wirasantosa, F. Qiao, A. Supangat, B. Fan, Z. Wei, B. Sulistiyo, and S. Li (2010), Volume, heat, and freshwater transports from the South China Sea to Indonesian seas in the boreal winter of 2007–2008, *J. Geophys. Res.*, *115*, C12020, doi:10.1029/2010JC006225.

Ffield, A., and A. L. Gordon (1992), Vertical mixing in the Indonesian thermocline, *J. Phys. Oceanogr.*, *22*, 184–195, doi:10.1175/1520-0485(1992)022<0184:VMITIT>2.0.CO;2.

Ffield, A., K. Vranes, A. L. Gordon, R. D. Susanto, and S. L. Garzoli (2000), Temperature variability within Makassar Strait, *Geophys. Res. Lett.*, *27*, 237–240, doi:10.1029/1999GL002377.

Gordon, A. L. (2005), Oceanography of the Indonesian seas and their throughflow, *Oceanography*, *18*, 14–27, doi:10.5670/oceanog.2005.01.

Gordon, A. L., and R. Fine (1996), Pathways of water between the Pacific and Indian Oceans in the Indonesian seas, *Nature*, *379*, 146–149, doi:10.1038/379146a0.

Gordon, A. L., R. D. Susanto, and A. Ffield (1999), Throughflow within Makassar Strait, *Geophys. Res. Lett.*, *26*, 3325–3328, doi:10.1029/1999GL002340.

Gordon, A. L., C. F. Giulivi, and A. G. Ilahude (2003a), Deep topographic barriers within the Indonesian seas, *Deep Sea Res., Part II*, *50*, 2205–2228, doi:10.1016/S0967-0645(03)00053-5.

Gordon, A. L., R. D. Susanto, and K. Vranes (2003b), Cool Indonesian throughflow as a consequence of restricted surface layer flow, *Nature*, *425*, 824–828, doi:10.1038/nature02038.

Gordon, A. L., R. D. Susanto, A. Ffield, B. A. Huber, W. Pranowo, and S. Wirasantosa (2008), Makassar Strait throughflow, 2004 to 2006, *Geophys. Res. Lett.*, *35*, L24605, doi:10.1029/2008GL036372.

Gordon, A. L., J. Sprintall, H. M. van Aken, R. D. Susanto, S. Wijffels, R. Molcard, A. Ffield, W. Pranowo, and S. Wirasantosa (2010), The Indonesian throughflow during 2004–2006 as observed by the INSTANT program, *Dyn. Atmos. Oceans*, *50*, 115–128, doi:10.1016/j.dynatmoce.2009.12.002.

Gordon, A. L., B. Huber, E. J. Metzger, R. D. Susanto, H. Hurlburt, and T. R. Adi (2012), South China Sea throughflow impact on the Indonesian throughflow, *Geophys. Res. Lett.*, *39*, L11602, doi:10.1029/2012GL052021.

Hautala, S., J. Sprintall, J. T. Potemra, J. C. Chong, W. Pandoe, N. Bray, and A. Ilahude (2001), Velocity structure and transport of the Indonesian throughflow in the major straits restricting flow into the Indian Ocean, *J. Geophys. Res.*, *106*, 19,527–19,546, doi:10.1029/2000JC000577.

Ilahude, A. G., and A. L. Gordon (1996), Thermocline stratification within the Indonesian seas, *J. Geophys. Res.*, *101*, 12,401–12,409, doi:10.1029/95JC03798.

Iskandar, I., W. Mardiansyah, Y. Masumoto, and T. Yamagata (2005), Intraseasonal Kelvin waves along the southern coast of Sumatra and Java, *J. Geophys. Res.*, *110*, C04013, doi:10.1029/2004JC002508.

Kashino, Y., A. Ishida, and S. Hosoda (2011), Observed ocean variability in the Mindanao dome region, *J. Phys. Oceanogr.*, *41*, 287–302, doi:10.1175/2010JPO4329.1.

McCreary, J. P. (1984), Equatorial beams, *J. Mar. Res.*, *42*, 395–430, doi:10.1357/002224084788502792.

McCreary, J. P., et al. (2007), Interactions between the Indonesian throughflow and circulations in the Indian and Pacific Oceans, *Prog. Oceanogr.*, *75*, 70–114, doi:10.1016/j.pocean.2007.05.004.

Metzger, E. J., H. E. Hurlburt, X. Xu, J. F. Shriver, A. L. Gordon, J. Sprintall, R. D. Susanto, and H. M. van Aken (2010), Simulated and observed circulation in the Indonesian seas: 1/12° global HYCOM and the INSTANT observations, *Dyn. Atmos. Oceans*, *50*, 275–300, doi:10.1016/j.dynatmoce.2010.04.002.

Meyers, G. (1996), Variation of Indonesian throughflow and the El Niño–Southern Oscillation, *J. Geophys. Res.*, *101*, 12,255–12,263, doi:10.1029/95JC03729.

Nagura, M., and M. J. McPhaden (2010), Wyrtki Jet dynamics: Seasonal variability, *J. Geophys. Res.*, *115*, C07009, doi:10.1029/2009JC005922.

Potemra, J. T., S. L. Hautala, J. Sprintall, and W. Pandoe (2002), Interaction between the Indonesian seas and the Indian Ocean in observations and numerical models, *J. Phys. Oceanogr.*, *32*, 1838–1854, doi:10.1175/1520-0485(2002)032<1838:IBTISA>2.0.CO;2.

Potemra, J. T., S. L. Hautala, and J. Sprintall (2003), Vertical structure of Indonesian throughflow in a large-scale model, *Deep Sea Res., Part II*, *50*, 2143–2161, doi:10.1016/S0967-0645(03)00050-X.

Pujiana, K., A. L. Gordon, J. Sprintall, and R. D. Susanto (2009), Intraseasonal variability in the Makassar Strait thermocline, *J. Mar. Res.*, *67*, 757–777, doi:10.1357/002224009792006115.

Pujiana, J., A. L. Gordon, E. J. Metzger, and A. L. Ffield (2012), The Makassar Strait pycnocline variability at 20–40 Days, *Dyn. Atmos. Oceans*, *53–54*, 17–35, doi:10.1016/j.dynatmoce.2012.01.001.

Qiu, B., M. Mao, and Y. Kashino (1999), Intraseasonal variability in the Indo-Pacific throughflow and the regions surrounding the Indonesian seas, *J. Phys. Oceanogr.*, *29*, 1599–1618, doi:10.1175/1520-0485(1999)029<1599:IVITIP>2.0.CO;2.

Qiu, Y., L. Li, and W. Yu (2009), Behavior of the Wyrtki Jet observed with surface drifting buoys and satellite altimeter, *Geophys. Res. Lett.*, *36*, L18607, doi:10.1029/2009GL039120.

Qu, T., J. Gan, A. Ishida, Y. Kashino, and T. Tozuka (2008), Semiannual variation in the western tropical Pacific Ocean, *Geophys. Res. Lett.*, *35*, L16602, doi:10.1029/2008GL035058.

Robertson, R. (2010), Tidal currents and mixing at the INSTANT mooring locations, *Dyn. Atmos. Oceans*, *50*, 331–373, doi:10.1016/j.dynatmoce.2010.02.004.

Saji, N. H., B. N. Goswani, P. N. Vinayachandran, and T. Yamagata (1999), A dipole mode in the tropical Indian Ocean, *Nature*, *401*, 360–363, doi:10.1038/43854.

Shinoda, T., E. J. Metzger, and H. Hurlburt (2011), Anomalous tropical ocean circulation associated with La Niña Modoki, *J. Geophys. Res.*, *116*, C12001, doi:10.1029/2011JC007304.

Shinoda, T., W. Han, E. J. Metzger, and H. Hurlburt (2012), Seasonal variation of the Indonesian throughflow in Makassar Strait, *J. Phys. Oceanogr.*, *42*, 1099–1123, doi:10.1175/JPO-D-11-0120.1.

Shriver, J. F., H. E. Hurlburt, O. M. Smedstad, A. J. Wallcraft, and R. C. Rhodes (2007), 1/32° real-time global ocean prediction and value-added over 1/16° resolution, *J. Mar. Syst.*, *65*, 3–26, doi:10.1016/j.jmarsys.2005.11.021.

Sprintall, J., J. Chong, F. Syamsudin, W. Morawitz, S. Hautala, N. Bray, and S. Wijffels (1999), Dynamics of the South Java current in the Indo-Australian Basin, *Geophys. Res. Lett.*, *26*, 2493–2496, doi:10.1029/1999GL002320.

Sprintall, J., A. L. Gordon, R. Murtugudde, and R. D. Susanto (2000), A semiannual Indian Ocean forced Kelvin wave observed in the Indonesian seas in May 1997, *J. Geophys. Res.*, *105*, 17,217–17,230, doi:10.1029/2000JC900065.

Sprintall, J., S. Wijffels, A. L. Gordon, A. L. Ffield, R. Molcard, R. D. Susanto, I. Soesilo, J. Sopaheluwakan, Y. Surachman, and H. M. van Aken (2004), INSTANT: A new international array to measure the Indonesian throughflow, *Eos Trans. AGU*, *85*(39), 369, doi:10.1029/2004EO390002.

Sprintall, J., S. E. Wijffels, R. Molcard, and I. Jaya (2009), Direct estimates of the Indonesian throughflow entering the Indian Ocean: 2004–2006, *J. Geophys. Res.*, *114*, C07001, doi:10.1029/2008JC005257.

Susanto, R. D., and A. L. Gordon (2005), Velocity and transport of the Makassar Strait throughflow, *J. Geophys. Res.*, *110*, C01005, doi:10.1029/2004JC002425.

Susanto, R. D., Q. Zheng, and X.-H. Yan (1998), Complex singular value decomposition analysis of equatorial waves in the Pacific observed by TOPEX/Poseidon altimeter, *J. Atmos. Oceanic Technol.*, *15*, 764–774, doi:10.1175/1520-0426(1998)015<0764:CSVDAO>2.0.CO;2.

Susanto, R. D., A. L. Gordon, J. Sprintall, and B. Herunadi (2000), Intraseasonal variability and tides in Makassar Strait, *Geophys. Res. Lett.*, *27*, 1499–1502, doi:10.1029/2000GL011414.

Susanto, R. D., A. L. Gordon, and Q. Zheng (2001), Upwelling along the coasts of Java and Sumatra and its relation to ENSO, *Geophys. Res. Lett.*, *28*(8), 1599–1602, doi:10.1029/2000GL011844.

Susanto, R. D., G. Fang, I. Soesilo, Q. Zheng, F. Qiao, Z. Wei, and B. Sulistyo (2010), New surveys of a branch of the Indonesian throughflow, *Eos Trans. AGU*, *91*(30), 261, doi:10.1029/2010EO300002.

Syamsudin, F., A. Kaneko, and D. B. Haidvogel (2004), Numerical and observational estimates of Indian Ocean Kelvin instrusion into Lombok Strait, *Geophys. Res. Lett.*, *31*, L24307, doi:10.1029/2004GL021227.

Tozuka, T., T. Qu, and T. Yamagata (2007), Dramatic impact of the South China Sea on the Indonesian throughflow, *Geophys. Res. Lett.*, *34*, L12612, doi:10.1029/2007GL030420.

Tozuka, T., T. Qu, Y. Masumoto, and T. Yamagata (2009), Impacts of the South China Sea throughflow on seasonal and interannual variations of the Indonesian throughflow, *Dyn. Atmos. Oceans*, *47*, 73–85, doi:10.1016/j.dynatmoce.2008.09.001.

van Aken, H. M., I. S. Brodjonegoro, and I. Jaya (2009), The deep-water motion through the Lifamatola passage and its contribution to the Indonesian throughflow, *Deep Sea Res., Part I*, *56*, 1203–1216, doi:10.1016/j.dsr.2009.02.001.

Vinayachandran, P. N., J. Kurian, and C. P. Neema (2007), Indian Ocean response to anomalous conditions in 2006, *Geophys. Res. Lett.*, *34*, L15602, doi:10.1029/2007GL030194.

Wajsowicz, R. C. (1996), Flow of a western boundary current through multiple straits: An electrical circuit analogy for the Indonesian throughflow and archipelago, *Geophys. Res. Lett.*, *101*, 12,295–12,300, doi:10.1029/95JC02615.

Wajsowicz, R. C., A. L. Gordon, A. Ffield, and R. D. Susanto (2003), Estimating transport in Makassar Strait, *Deep Sea Res., Part II*, *50*, 2163–2181, doi:10.1016/S0967-0645(03)00051-1.

Webster, P. J., A. M. Moore, J. P. Loschnigg, and R. R. Leben (1999), Coupled ocean–atmosphere dynamics in the Indian Ocean during 1997–1998, *Nature*, *401*, 356–360, doi:10.1038/43848.

Wheeler, M. C., and J. L. McBride (2005), Australian-Indonesian monsoon, in *Intraseasonal Variability in the Atmosphere–ocean System*, edited by W. K. M. Lau and D. E. Waliser, chap. 5, pp. 125–173, Springer, Berlin, doi:10.1007/3-540-27250-X_5.

Wijffels, S., E. Firing, and J. Toole (1995), The mean structure and variability of the Mindanao Current at 8°N, *J. Geophys. Res.*, *100*, 18,421–18,435, doi:10.1029/95JC01347.

Wyrtki, K. (1973), An equatorial jet in the Indian Ocean, *Science*, *181*, 262–264, doi:10.1126/science.181.4096.262.

Wyrtki, K. (1987), Indonesian throughflow and the associated pressure gradient, *J. Geophys. Res.*, *92*(C12), 12,941–12,946, doi:10.1029/JC092iC12p12941.